Lasers in Manufacturing Conference 2015

Properties of steel-aluminum joints generated by combining continuous and pulsed laser radiation

Sascha Frank[a], Kristian Arntz[a,]*, Fritz Klocke[a]

[a]*Fraunhofer Institute for Production Technology IPT, Steinbachstr. 17, 52074 Aachen, Germany*

Abstract

The combination of a continuous and a pulsed laser beam in a common process zone makes it possible to join aluminum and galvanized steel. This method does not require the use of chemical fluxes. It can be applied to different joint geometries such as double-flanged joints and lap joints. The basic microstructure of these joints is discussed using metallographic cross-sections. The properties of the intermetallic iron-aluminum compounds are examined in greater detail using methods such as energy-dispersive X-ray spectroscopy (EDS) and transmission electron microscopy (TEM). The results from these measurements indicate that the use of wire material alloys containing silicon leads to the formation of ternary phases. The joints exhibit a high strength in mechanical tests even when cyclic loads are applied.

Keywords: Laser joining; welding; brazing; hybrid; galvanized steel; aluminium; zinc; mixed-metal joints

1. Introduction

Lightweight design is a key technology for achieving lower energy consumption and improved product performance in many areas of industrial manufacturing. However, high costs often prevent the use of exotic lightweight materials like carbon fiber reinforced plastics in mass-market applications. Steel-aluminum mixed-metal systems offer a more cost-efficient solution. Yet, few established technologies are suitable for joining these dissimilar metals due to their high tendency to form intermetallic compounds (IMCs). IMCs can severely reduce the strength of a joint due to their high brittleness. However, as shown by Laukant, 2007, the joint will possess good mechanical properties if the intermetallic layer at the interface between both

* Corresponding author. Tel.: +49-241-8904-121; fax: +49-241-8901-6121.
E-mail address: kristian.arntz@ipt.fraunhofer.de.

materials can be limited to a non-critical thickness of less than 10 µm. This can be achieved by minimizing the temperature of the joining process as well as its duration.

This goal can be achieved by employing a joining process in which two different laser beams are combined. The basic setup for this combined process is shown in Fig. 1 (a). As in conventional brazing, the method involves the use of a laser source operating in continuous wave (cw) mode and a consumable brazing wire. The cw beam is shaped to a circular spot. It is combined with an additional pulsed (pw) laser beam, which is used to destroy the highly resistant oxide layer of the aluminum materials. This makes it possible to achieve good wetting conditions at low cw output powers without having to employ chemical fluxing agents. The pw beam possesses a line-shaped focus in order to minimize the focal area while still allowing the pw laser to affect the whole width of the seam. The process requires the use of shield gas, which is supplied via a tube not shown in the image.

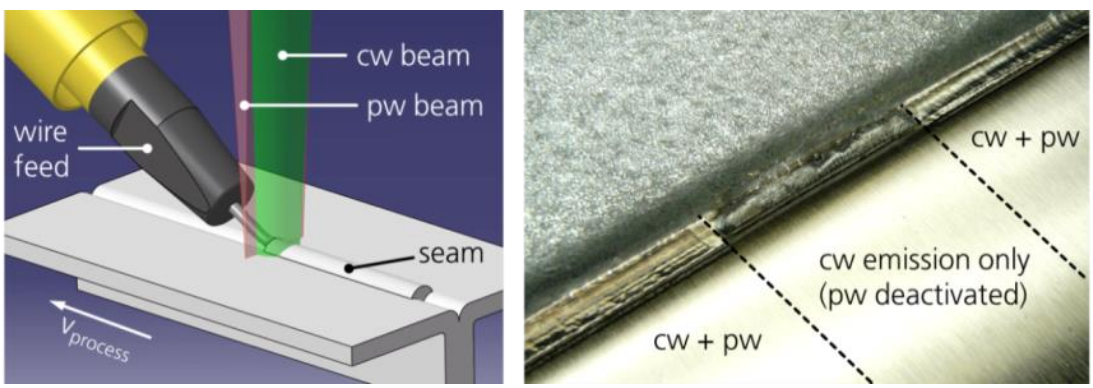

Fig. 1. (a) 3D illustration of the basic process setup; (b) sample seam demonstrating the effect of the pulsed laser

A sample seam which illustrates the process principle is shown in Fig. 1 (b). The sample possesses a double-flanged geometry. It was created at a process speed of v_{join} = 0.7 m/min and average output powers of P_{cw} = 1.1 kW and P_{pw} = 58 W. The wire was supplied at a speed of v_{wire} = 1.2 m/min. During the process, the pw laser was deactivated for a short distance, while the cw laser remained active. As shown by the image, this led to a complete interruption of the joining process, even though the average output power of the cw laser of was significantly larger than that of the pw source. While the pw laser was deactivated, the thermal energy generated by the cw radiation was not sufficient to destroy the oxide layer of the wire material. In consequence, the wire retained its shape and was barely fused to the base materials. As also shown by the image, the joining process immediately re-stabilized once the pw laser was reactivated.

2. Basic microstructure

Mixed-metal joints between aluminum and galvanized steel can be created using either zinc-based or aluminum-based consumables. The joining method described in this paper is suitable for processing both types of wire materials, as shown by Frank, 2015. The most promising results were achieved using the wire alloys AlSi5, AlSi12 and ZnAl2. The method has also been tested successfully on several different base materials. This includes the aluminum alloys AlMgSi1 and AlMg3 as well as the galvanized steel alloys DC04+ZE75/75 and DX51D+Z275. Fig. 2 shows an example in which the materials AlMg3 and DX51D+Z were joined in an overlapping configuration at a process speed of v_{join} = 0.7 m/min.

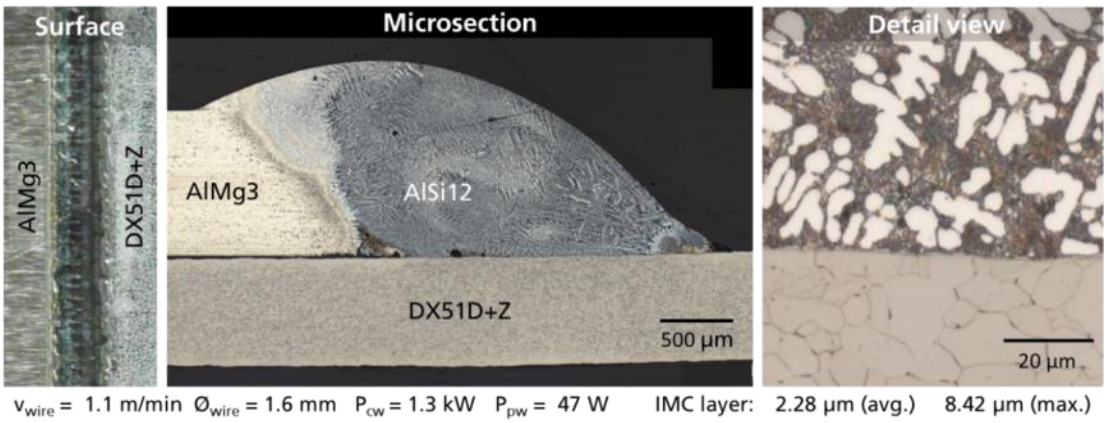

Fig. 2. Microstructure of a lap joint created using the combined process

The seam shown in the image demonstrates that the joining method can not only be applied to double-flanged joints, but also to lap joints. The surface is smooth and even. The microsection reveals a high joint quality. While the aluminum sheet was fully fused, the connection to the galvanized steel was established by brazing. The connection length to the steel sheet exceeds the thickness of the aluminum material. The detail view shows only a very thin intermetallic layer, which is barely discernable in the image. Its average thickness was determined to be 2.28 µm. However, the maximum thickness reaches a value of 8.42 µm due to several isolated spikes protruding from this layer. This value still falls below the guideline value of 10 µm.

Fig. 3 shows another test seam, which was joined at an elevated process speed of v_{join} = 1.8 m/min. In order to be able to increase the process speed, the cw output power was also increased. Compared to the example given in Fig. 1 (b), the power of the pw laser was slightly decreased. In total, this led to a more beneficial ratio of laser power to process speed. Again, the pw laser was deactivated during the joining process. Despite the lower P_{cw}/v_{join} and P_{cw}/v_{wire} ratios, the higher power of the cw laser proved sufficient to melt a large portion of the filler wire in this case. However, both the surface view and the cross-sectional view of the seam show a severe degradation of the wetting conditions after the deactivation of the pw laser.

The microsection of the first segment, which was joined using both laser beams, shows a good joint quality. The seam surface is concave and the material transition to both base materials is near-tangential. Due to the thick zinc coating of the DX51D+Z275 material and the high laser output power, the joint contains a low amount of porosity in the area where the seam root meets the steel material. An IMC layer is barely discernable in the detail view. The second section, which was created using only the cw laser, shows a severe degradation of quality. The seam surface is less regular and the porosity of the seam is significantly higher. Due to the high amount of porosity, the connection length to the aluminum material is very short. The convexity of the seam root is higher. Even though the total amount of laser energy absorbed by this second section of the seam is lower, the detail view shows a much stronger growth of intermetallic compounds. The shape of these compounds is very angular and crystalline. In addition, the microsection contains a large amount of needle-shaped structures, some of which are marked by arrows in the detail view.

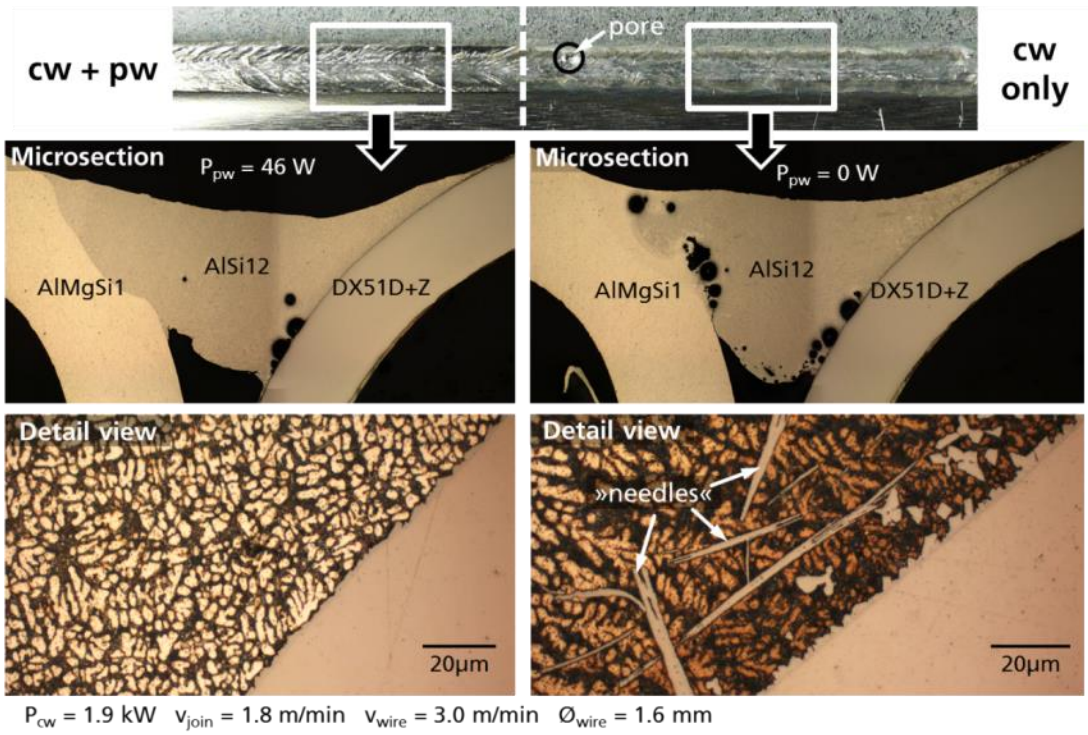

Fig. 3. Effect of pulsed laser at elevated process speed and cw power

This example again demonstrates the fact that the additional effect of the pw laser can strongly improve the seam quality in comparison to a single-beam process. However, the needle-like structures observed in the second section of the seam have also been found in microsections of seams generated by using both lasers, albeit in smaller amounts. The occurrence of needle-shaped compounds was predominantly registered when AlSi12 was used as a consumable. They did not occur in experiments with zinc-based consumables.

3. TEM analysis

In order to gain further insight into the composition of these mixed-metal joints, selected samples were examined via transmission electron microscopy (TEM). TEM analysis offers the advantage of high precision and very high possible resolutions. However, each analysis requires the elaborate preparation of a microscopic lamella via focused ion beam (FIB). Two such lamellae were prepared from a sample, in which the presence of needle-shaped microstructural components had been determined. The sample was created by depositing AlSi12 material in a bead-on-plate configuration on DX51D+Z using combined pw and cw laser radiation. Fig. 4 shows both lamellae, including their previous location in the sample. The lamellae were extracted vertically from the plane shown in the middle image. This makes it possible to gain a 3-dimensional impression of the microstructure. By comparing the images shown in Fig. 5, it becomes apparent that the structures being examined only possess a needle-like shape in a two-dimensional view. In fact, they are actually shaped like platelets.

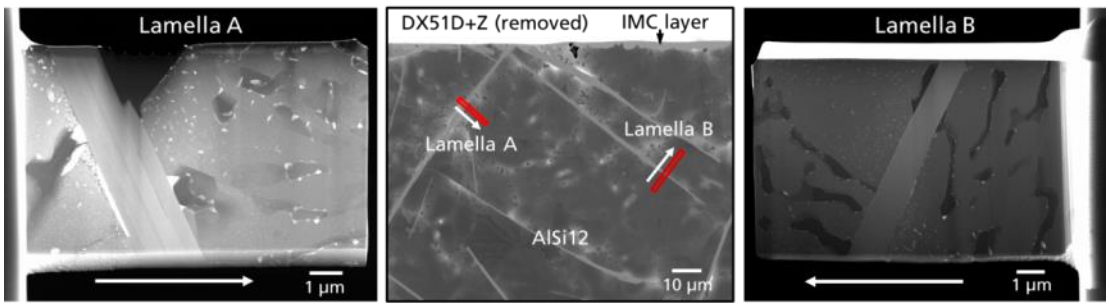

Fig. 4. Preparation of TEM lamellae from a larger sample via FIB

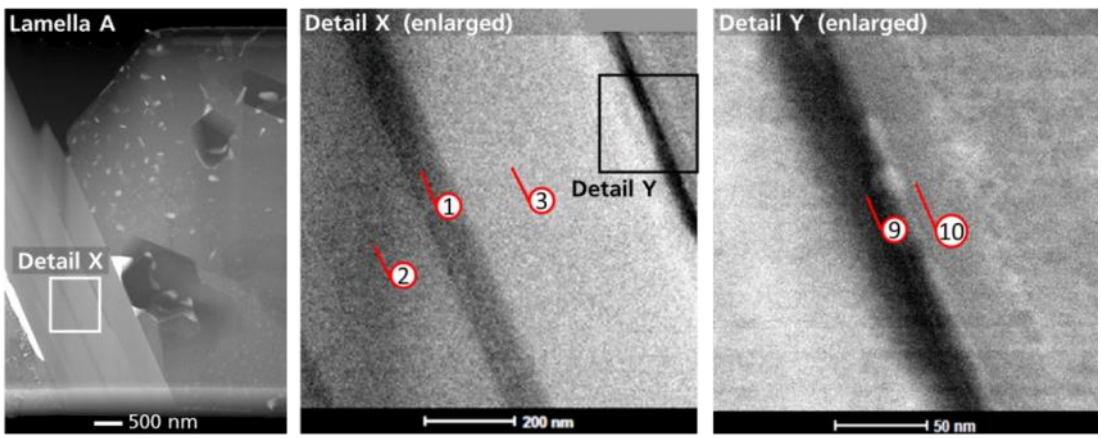

Fig. 5. Analysis of needle-like microstructural components

Fig. 5 shows enlarged views of the platelets in lamella A. To gain more information about these platelets, their composition was measured using energy-dispersive X-ray spectroscopy (EDS). Measurements were performed on both lamellae using the EDS detector of the TEM. Additional measurements were made using a scanning electron microscope (SEM). The results are listed in table 1. The location of five of these measurements is marked in Fig. 5. These measurements were performed as line scans. The results in the table are highlighted in different colors according to similar composition. As the table shows, most of these measurements delivered almost identical values. The measurements made via SEM are well in agreement with those taken by TEM. Table 2 shows the average values of these groups in direct comparison to the composition of several ternary phases from the Fe-Al-Si system.

The Fe-Al-Si system contains a high amount of different intermetallic compounds. Their identification is complicated by the similar composition of some of these phases. Additional challenges result from the potential presence of meta-stable phases and slow-running peritectic transformations. Also, it must be considered that literature values for the composition of intermetallic compounds are often based on diffusion-based long-time experiments. An example for this are the diffusion experiments performed by Krendelsberger et al., 2007, which involved heat treatments lasting up to 1 month. The timescale of these experiments differs significantly from that of a laser joining operation.

Table 1. Composition of IMC platelets

	Reference No.	Method / scan type	Wire material	Al (At %)	Si (At %)	Fe (At %)	Zn (At %)
1	A14L1	TEM / line	AlSi12	66.2	15.9	17.7	0.2
2	A14L2	TEM / line	AlSi12	57.1	23.2	19.7	0.0
3	A14L3	TEM / line	AlSi12	56.9	23.4	19.6	0.0
4	B12A1	TEM / area	AlSi12	66.1	16.7	17.1	0.1
5	A25A1	TEM / area	AlSi12	56.8	24.2	18.9	0.0
6	A25L1	TEM / line	AlSi12	49.3	36.7	13.5	0.5
7	A25L2	TEM / line	AlSi12	67.9	14.7	16.7	0.6
8	A25A2	TEM / area	AlSi12	65.3	15.8	18.1	0.7
9	A15L1	TEM / line	AlSi12	48.5	35.3	15.3	0.8
10	A15L2	TEM / line	AlSi12	64.2	14.1	20.6	1.0
11	A13P3	TEM / area	AlSi12	69.8	13.7	15.7	0.7
12	323P1	SEM / point	AlSi12	69.1	17.6	13.0	0.2
13	323P2	SEM / point	AlSi12	70.2	17.5	11.9	0.3
14	323P3	SEM / point	AlSi12	74.5	15.0	10.2	0.3
15	661-2	SEM / point	AlSi5	63.8	19.3	14.3	2.6
16	664-55	SEM / point	AlSi5	62.4	21.9	10.6	5.1
17	664-60	SEM / point	AlSi5	66.9	20.2	8.9	4.0
18	664-61	SEM / point	AlSi5	66.0	19.5	11.0	3.5

Table 2. Average results and composition of selected intermetallic compounds

Composition	Short sign	Al (At %)	Si (At %)	Fe (At %)	Zn (At %)
Avg. (light grey)		48.9	36.0	14.4	0.6
Al3FeSi2	τ4	50.0	33.3	16.7	0.0
Avg. (dark grey)		56.9	23.6	19.4	0.0
Al3FeSi	τ2	60.0	20.0	20.0	0.0
Avg. (white)		67.1	17.1	14.3	1.5
AL4FeSi	τ6	66.7	16.7	16.7	0.0
Al4.5FeSi	τ6	69.2	15.4	15.4	0.0

The occurrence of similar needle-like compounds in multi-material joints has previously been reported by Laukant, 2007 and Thomy et al., 2007. According to Laukant, the formation of these needle-like structures does not reduce the joint strength. Both sources identified the composition of these compounds as FeAl3. However, according to Maitra and Gupta, 2003, the solubility of Si in FeAl3 amounts to less than 6 %. As shown by the data in table 1, the measurements showed Si concentrations of 13 - 22 at%. Despite this result, the phase appears homogeneous even at a nanoscopic scale (cf. Fig. 5). This result contradicts the classification of this phase as FeAl3. However, the comparison in table 2 shows that the majority of the

results correspond well to the nominal composition of the τ6 phase. Depending on the source, this phase is identified as Al4FeSi (Maitra and Gupta, 2003) or Al4.5FeSi (Krendelsberger et al., 2007). According to Maitra and Gupta, this phase also forms needle- or plate-like structures. By conclusion, it is highly likely that the examined platelets are formed by the τ6 phase. This conclusion is supported by the fact that compounds of this type were most often observed with use of AlSi12 wire material, which contains a high amount of Si, but never with zinc-based alloys like ZnAl2, which do not contain a significant amount of Si. In addition, the TEM images show that the τ6 phase is interspersed with low amounts of τ2 and τ4.

The analysis of the platelet-shaped compounds has led to the conclusion that the use of consumables containing silicon can induce the growth of ternary Fe-Al-Si phases. However, this effect is not necessarily limited to platelet-shaped compounds. It may also affect the continuous layer of intermetallic compounds which forms along the interface to the steel material. To examine whether this layer also contains ternary compounds, its composition was also evaluated by SEM and TEM. One of the lamellae from these analyses is shown in Fig. 6, including a magnified view of the IMC layer. The detail view shows that the IMC layer possesses a homogeneous structure. It also shows the location of two area scans. The results of these scans are provided in table 3 along with the results of other measurements of the IMC layer composition.

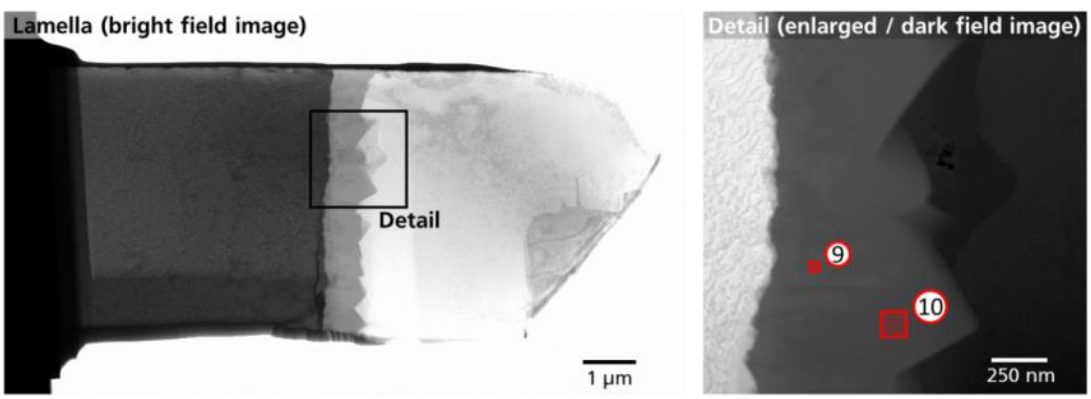

Fig. 6. TEM analysis of IMC layer

The table shows only a small amount of variation in the data. Along with the homogeneous structure of the IMC layer, this suggests that it consists of a single phase with a predefined range of existence. A list of phases of similar nominal composition is given in table 4. In addition to the τ6 phase, two different compositions are also listed for τ5, which are based on the analyses by Krendelsberger et al., 2007 and Raghavan, 2002. This discrepancy again shows that the evaluation of the ternary Fe-Al-Si system is still an ongoing process. This circumstance is further illustrated the fact that different literature sources also provide different versions of the phase diagrams for this system. For example, the liquidus projections published by Krendelsberger et al. and Raghavan show differently shaped areas for those phases common to both projections while assuming a different amount of phases in other areas of the diagram.

The first item listed in the table is the binary phase Al5Fe2. This phase commonly forms during hot dip galvanizing if the aluminum content of the zinc bath exceeds 0.15 wt%, as stated by Marder, 2000. For this reason, it is likely that a joint between aluminum and galvanized steel will also contain this phase. However, according to Maitra and Gupta, 2003, the maximum solubility of silicon in Al5Fe2 is only 7.57 at%. The

resulting composition of an Al5Fe2 phase, which is fully saturated with Si, is also given in table 4. As shown by table 3, the silicon content exceeds the limit of 7.5 at% in almost all measurements. While some authors, such as Liu and Chang, 1999 indicate that the solubility may be even higher, the possibility that the IMC layer consists of a ternary phase must also be considered. As shown by the comparison in table 4, the composition of the IMC layer is highly congruent with that of the Al7.4Fe2Si (τ5) phase.

Table 3. Composition of IMC layer

	Reference No.	Method / scan type	Wire material	Al (At %)	Si (At %)	Fe (At %)	Zn (At %)
1	664-8	SEM / point	AlSi12	63.8	10.3	23.3	2.6
2	664-9	SEM / point	AlSi12	67.7	10.0	18.8	3.5
3	664-10	SEM / point	AlSi12	68.1	10.7	18.3	2.9
4	451-5	SEM / point	AlSi12	66.0	13.9	20.1	0.0
5	451-6	SEM / point	AlSi12	69.6	14.9	14.6	0.9
6	865-2-2	TEM / area	AlSi12	67.1	11.5	20.5	0.4
7	1020-2	TEM / area	AlSi5	68.5	10.3	20.0	0.0
8	1020-3	TEM / area	AlSi5	70.1	9.7	18.5	0.0
9	820-3-1	TEM / area	AlSi5	69.2	7.0	23.7	0.0
10	820-3-2	TEM / area	AlSi5	69.4	10.2	19.7	0.7
11	820-5-1	TEM / area	AlSi5	68.1	9.9	21.0	0.5
12	820-5-2	TEM / area	AlSi5	70.6	9.1	19.3	0.7

Table 4. Average result of IMC layer analysis and composition of selected intermetallic compounds

Composition	Short sign	Al (At %)	Si (At %)	Fe (At %)	Zn (At %)
Avg. (IMC layer)		68.2	10.6	19.8	1.0
Al5Fe2		71.4	0.0	28.6	0.0
Al5Fe2 + 7.5% Si		66.1	7.5	26.4	0.0
Al7.4Fe2Si	τ5	71.1	9.6	19.2	0.0
Al15Fe6Si5	τ5	57.7	19.2	23.1	0.0
Al4FeSi	τ6	66.7	16.7	16.7	0.0
Al4.5FeSi	τ6	69.2	15.4	15.4	0.0

The platelet-shaped compounds, which have been correlated with the τ6 phase, possess a high average silicon content of 17.1 at%. They have most often been observed when the wire material AlSi12 was used, which also contains a high percentage of Si. This suggests that wire materials containing a high amount of Si may facilitate the growth of ternary compounds. To examine this theory, table 5 shows another comparison of the measurements presented in tables 1 and 5. The average values are now correlated to the wire materials. The measurements taken from the IMC layer show a higher Si-content when AlSi12 was used. However, the Si-percentage of the platelets was higher for the wire material AlSi5. Contrary to the initial expectations, these results indicate that the Si content of the wire material is not directly related to the Si

content of the intermetallic compounds. However, as has been shown previously by Frank, 2015, the IMC layer will not contain a notable amount of silicon when zinc-based alloys like ZnAl2 are used.

Table 5. Average composition of IMCs in dependence of the wire material

IMC type	Wire material	Al (At %)	Si (At %)	Fe (At %)	Zn (At %)
Platelets (τ6)	AlSi5+AlSi12	67.1	17.1	14.3	1.5
	AlSi12	68.1	15.7	15.7	0.5
	AlSi5	64.8	20.2	11.2	3.8
IMC layer (τ5)	AlSi5+AlSi12	68.2	10.6	19.8	1.0
	AlSi12	67.1	11.9	19.3	1.7
	AlSi5	69.3	9.4	20.4	0.3

4. Mechanical strength

The mechanical properties of a mixed-metal joint are strongly influenced by its microstructure. As has been shown by Frank, 2015, steel-aluminum joints created by using the combined laser process can reach a strength of up to 232.1 MPa. However, the quasi-static stress applied in tensile tests only leads to limited conclusions about the brittleness of a joint. In consequence, the joint behavior was also tested under cyclic loads. The cyclic load tests were performed on two sets of samples which were joined using AlSi5 and AlSi12. The sample geometry is shown in Fig.7. The tests were performed at a frequency of 760 Hz. As demonstrated by the samples shown in the image, base material failure could be achieved using both types of consumables. The image of the AlSi12 sample shows that mixed-mode failure is also possible, where a crack simultaneously occurs in both seam and base material.

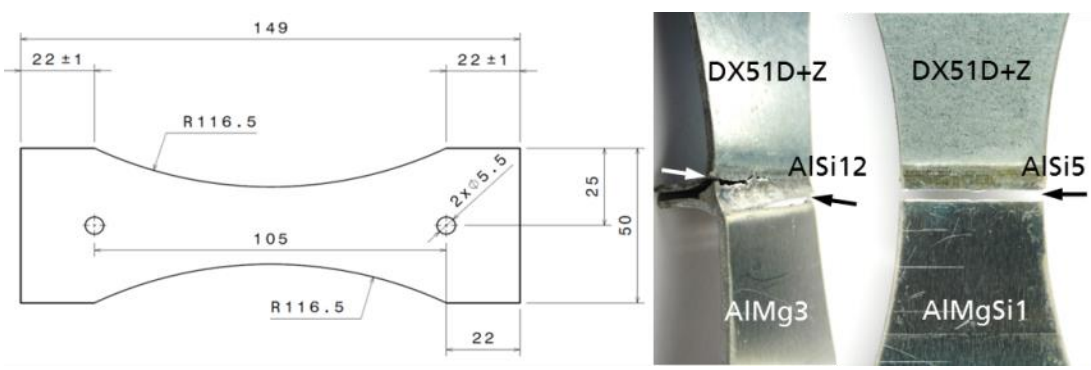

Fig. 7. (a) sample geometry for cyclic load tests; (b) examples of fractured samples exhibiting base material failure

Fig. 8 shows a diagram representing the results of the cyclic load tests. The material stress was calculated using the nominal cross-section of the aluminum sheet. The diagram shows that a higher amount of cycles could be reached using AlSi5. The diagram also contains two lines of best fit, which were calculated logarithmically. Both lines show an increase of sample life with decreasing stress. However, a larger amount of samples would be required to generate more conclusive results. Samples where failure occurred within the base material are marked with a dark outline, showing that the majority of samples failed in this mode.

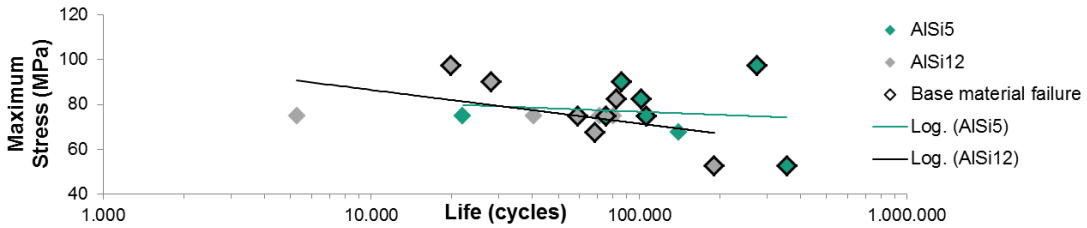

Fig. 8. Results of cyclic load tests

5. Conclusions

- By superimposing a pulsed and a continuous laser beam, it becomes possible to create mixed-metal joints at low cw output powers. Even if the power of the cw laser is high enough to fuse the wire material, the microstructure can be improved by also employing the pw laser.
- Steel-aluminum joints may contain intermetallic compounds which exhibit a needle-like shape in 2-dimensional microsections. The preparation of TEM-samples by focused ion beam has shown that these compounds actually possess the shape of platelets.
- The results indicate that these platelets correspond to the τ6 phase of the ternary Fe-Al-Si system.
- The use of Al-Si-based wire alloys also leads to a high Si content in the intermetallic layer. This layer may also consist of ternary phases, the most likely of which is the τ5 phase.
- The Si content of the intermetallic layer shows no direct relation to the Si content of the wire material.
- The joints possess a high strength. Base material failure can even be achieved under cyclic loads.

Acknowledgements

The German Federal Ministry of Education and Research (BMBF) is gratefully acknowledged for financial support of the project »FerroPuls«, grant No. 03V0203, on which this publication is based. The responsibility for the contents of this publication lies with the author.

References

Frank, S., 2015. Flux-free laser joining of aluminum and galvanized steel. Journal of Materials Processing Technology 222, p. 365-372

Krendelsberger, N., Weitzer, F., Schuster, J.C., 2007. On the Reaction Scheme and Liquidus Surface in the Ternary System Al-Fe-Si, Metallurgical and materials transactions 38A, p. 1687-1691

Laukant, H., 2007. Laserschweiß-Löten von Stahl-Aluminium-Mischverbindungen: Mechanisch-technologisches Eigenschaftsprofil und mikrostrukturelle Charakterisierung, Diss., Universität Bayreuth, p. 107-108.

Liu, Z.-K., Chang, Y.A., 1999. Thermodynamic Assessment of the Al-Fe-Si System, Metallurgical and materials transactions 30A, p. 1081-1095

Maitra, T., Gupta, S.P., 2003. Intermetallic compound formation in Fe–Al–Si ternary system: Part II, Materials Characterization 49, p. 293-311

Marder, A.R., 2000. The metallurgy of zinc-coated steel, Progress in Materials Science 45, p. 217

Raghavan, V., 2002. Al-Fe-Si (Aluminum-Iron-Silicon), Journal of Phase Equilibria Vol. 23 No. 4, p. 362-366

Thomy, C., Wagner, F., Vollertsen, F., Wirth, A., Kreimeyer, M., 2007. Laser-MIG-Hybridfügen von Aluminium-Stahl Leichtbaustrukturen, Laser Technik Journal 4, p. 38.